Journal of Alloys and Compounds 509 (2011) 3677–3681

Contents lists available at ScienceDirect

Journal of Alloys and Compounds

journal homepage: www.elsevier.com/locate/jallcom

Resistivity, thermopower, and thermal conductivity of nickel doped compounds $Cr_{1-x}Ni_xSb_2$ at low temperatures

Hai Jin Li[a,b], Xiao Ying Qin[b,*], Yi Liu[a], Di Li[b], Jin Lian Hu[c]

[a] School of Mathematics and Physics, Anhui University of Technology, Ma'anhan 243002, PR China
[b] Key Laboratory of Materials Physics, Institute of Solid State Physics, Chinese Academy of Science, Hefei 230031, PR China
[c] School of Materials Science and Engineering, and Anhui Key Laboratory of Metal Materials and Processing, Anhui University of Technology, Ma'anhan 243002, PR China

ARTICLE INFO

Article history:
Received 5 September 2010
Received in revised form
20 December 2010
Accepted 21 December 2010
Available online 28 December 2010

Keywords:
$Cr_{1-x}Ni_xSb_2$
Electrical resistivity
Thermopower
Thermal conductivity

ABSTRACT

Substitutional compounds $Cr_{1-x}Ni_xSb_2$ ($0 \le x \le 0.1$) were synthesized, and the effect of Ni substitution on transport and thermoelectric properties of $Cr_{1-x}Ni_xSb_2$ were investigated at the temperatures from 7 to 310 K. The results indicated that the magnitudes of the resistivity and thermopower of $Cr_{1-x}Ni_xSb_2$ decreased greatly with increasing Ni content at low temperatures, owing to an increase in electron concentration caused by Ni substitution for Cr. Experiments also showed that the low-temperature lattice thermal conductivity of $Cr_{1-x}Ni_xSb_2$ decreased substantially with increasing Ni content due to an enhancement of phonon scattering by the increased number of Ni atoms. As a result, the figure of merit, ZT, of lightly doped $Cr_{0.99}Ni_{0.01}Sb_2$ was improved at $T > \sim 230$ K. Specifically, the ZT of $Cr_{0.99}Ni_{0.01}Sb_2$ at 310 K was approximately ~29% larger than that of $CrSb_2$, indicating that thermoelectric properties of $CrSb_2$ can be improved by an appropriate substitution of Ni for Cr.

1. Introduction

Thermoelectric (TE) materials have recently attracted more and more attentions in the past decade due to their potential applications to refrigerators and electric-power generators [1]. The conversion efficiency of TE materials is represented by the dimensionless figure of merit, $ZT = S^2T/\rho\kappa$, where S, ρ, κ and T are the thermopower, the electrical resistivity, the thermal conductivity and the absolute temperature, respectively. Thus, high S, low κ, and small ρ are necessary for a good TE material. Although, several classes of materials that are currently under investigation include Bi–Sb–Te-based materials [2–6], PbTe-based materials [7–9], Zn_4Sb_3-based materials [10–13], Heusler alloys [14–16], skutterudites [17–19], metal oxides [20–23], clathrate compounds [24,25], and pentatellurides [26], their thermoelectric performance does not meet the requirements of large-scale industrial applications.

Recently, thermoelectric properties of $CrSb_2$ are investigated because of its high thermopower ($\sim|-431|\,\mu V\,K^{-1}$ at ~60 K) [27–29]. $CrSb_2$ has an orthorhombic marcasite structure (space group *Pnnm*) [30]. In this structure, each Cr atom has a distorted octahedral coordination of six nearest-neighbor Sb atoms; each Sb atom is tetrahedrally coordinated by three Cr atoms and one Sb atom, which needs 14 electrons to form the covalent bond. As a result, the left two unpaired electrons of each Cr atom do not participate in the covalent bonding, leading to a localized high-spin configuration with a d-state manifold per Cr atom $3d^2$ in $CrSb_6$-octahedron [31–33]. As an anti-ferromagnetic intermetallic compound, $CrSb_2$ has a Neel temperature of $T_N = 273 \pm 2$ K [34], which decreases monotonically with partial substitution of Cr by Fe [35]. A plateau of electrical resistivity locates in the temperature range from 50 to 80 K in the curve of $\ln\rho$ versus $1000/T$ and a sharp peak appears at approximately ~55 K in the curve of magnetic susceptibility χ versus temperature for $CrSb_2$, implying that an electronic change may occur in the electron-spin system [36,37]. The partial substitution of Cr by Ru leads to an increase in the thermopower $|S|$ and resistivity ρ of $Cr_{1-x}Ru_xSb_2$ at room temperature [38]. Moreover, $CrSb_2$ is a narrow-gap semiconductor with an energy gap of 0.07 eV [31,38], suggesting that $CrSb_2$ would be a potential thermoelectric material. Recently, we have studied the transport and thermoelectric properties of $CrSb_2$ after the substitution of Te, Sn, Mn, Ti for Cr, respectively [29,39–41]; and the ZT of $CrSb_{2-x}Te_x$, $Cr_{1-x}Mn_xSb_2$, and $Cr_{1-x}Ti_xSb_2$ were improved by an appropriate doping, however, the thermoelectric properties of $CrSb_{2-x}Sn_x$ were not optimized due to the decrease in the thermoelectric power factor ($PF = S^2T/\rho$). Additionally, the Neel temperature of $CrSb_2$ shifts to higher temperatures after Mn substitution, owing to the high spin $3d^3$ configuration of Mn [40]. In contrast, the change of Neel temperature could be negligible after Ti substitution due to neutral particles of Ti [41]. It is well known

* Corresponding author at: Institute of Solid State Physics, Chinese Academy of Science, P.O. Box: 1129, Hefei 230031, Anhui, PR China.
Tel.: +86 551 5592750; fax: +86 551 5591434.
E-mail address: xyqin@issp.ac.cn (X.Y. Qin).

0925-8388/$ – see front matter © 2011 Elsevier B.V. All rights reserved.
doi:10.1016/j.jallcom.2010.12.159

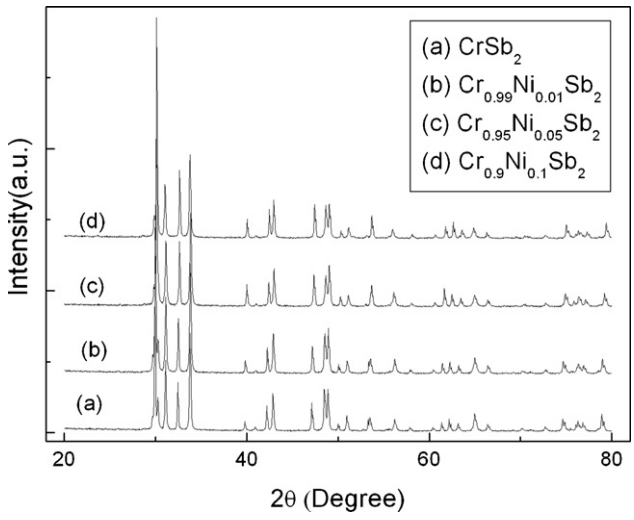

Fig. 1. XRD patterns (Cu Kα irradiation) for $Cr_{1-x}Ni_xSb_2$ (x = 0, 0.01, 0.05, and 0.10) at room-temperature.

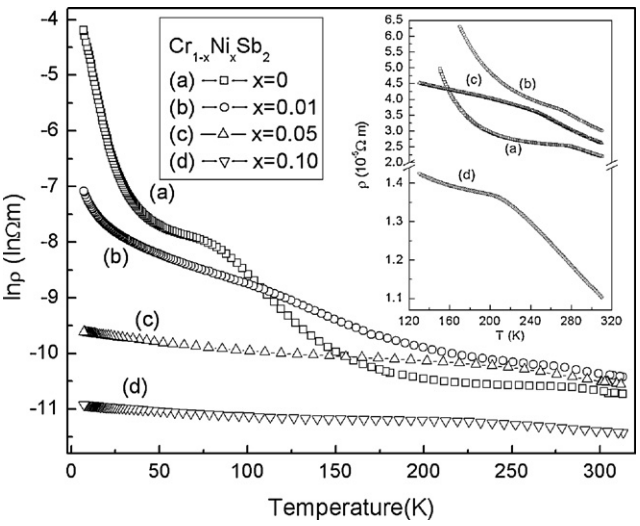

Fig. 3. Plot of the electrical resistivity ln ρ versus temperature T for $Cr_{1-x}Ni_xSb_2$ (x = 0, 0.01, 0.05, and 0.10). The inset shows variation of the electrical resistivity ρ with temperature T for $Cr_{1-x}Ni_xSb_2$ above 120 K.

that $NiSb_2$ and $CrSb_2$ have the same crystalline structure [30,42], furthermore, it is the low spin $3d^6$ configuration of Ni in $NiSb_2$ [32]. Thus, in the present work Ni doped compounds $Cr_{1-x}Ni_xSb_2$ were prepared, and their electrical resistivity (ρ), themopower (S) and thermal conductivity (κ) were investigated in the temperature range from 7 to 310 K.

2. Experimental methods

Polycrystalline samples of $Cr_{1-x}Ni_xSb_2$ (x = 0, 0.01, 0.05 and 0.10) were synthesized by the method of melting and alloying. Firstly, the mixtures of constituent elements Cr (purity: 99.9 at.%), Sb (purity: 99.9 at.%) and Ni (purity: 99.9 at.%) in stoichiometric proportions were sealed in evacuated quartz tubes under a pressure of approximately $\sim 2 \times 10^{-2}$ Pa. Then they were heated slowly to 650 °C and isothermally kept for 1 week to form $Cr_{1-x}Ni_xSb_2$ compounds. The phase structure of the obtained samples was examined using X-ray diffraction (XRD, Philips-X' Pert Pro) with Cu Kα irradiation. Accurate lattice parameters were determined from d-values of XRD peaks using the standard least-squares refinement method with an Si standard for calibration. To measure their transport properties, the synthesized $Cr_{1-x}Ni_xSb_2$ powders were compacted by hot pressing (under the pressure of 300 MPa) in vacuum at 400 °C for 60 min to form bulk samples. Bar-shaped specimens of with dimensions of ~13 mm × ~3 mm × ~1.5 mm were cut from the bulk samples. All transport properties (i.e. resistivity, thermopower, and thermal conductivity) were measured simultaneously using a physical property measurement system (PPMS, Quantum Design, USA) in the temperature range from 7 to 310 K. The carrier concentration was determined by measurements of the Hall coefficient at room temperature in a field, H = 0.73T.

3. Results and discussion

3.1. Phase determination and measurements of lattice parameters after Ni substitution

The XRD patterns of the $Cr_{1-x}Ni_xSb_2$ samples are shown in Fig. 1. It can be seen from curve (a) that all the main diffraction peaks correspond to those of standard JCPDS card of $CrSb_2$ with orthorhombic marcasite structure (space group *Pnnm*). As compared with that of pristine $CrSb_2$, no obvious changes are observed in the XRD patterns of the doped samples. The values of lattice parameters of $Cr_{1-x}Ni_xSb_2$ are calculated using the XRD data. As plotted in Fig. 2, the lattice parameters a, b and the volume of unit cell V of $Cr_{1-x}Ni_xSb_2$ decrease with increasing Ni content, whereas c increases, which are in agreement with the previous results [43,44]. In addition, the solid solubility limit of Ni in $CrSb_2$ is quite high due to the similar crystal structure of $CrSb_2$ to that of $NiSb_2$. These results indicate that Ni has suc-

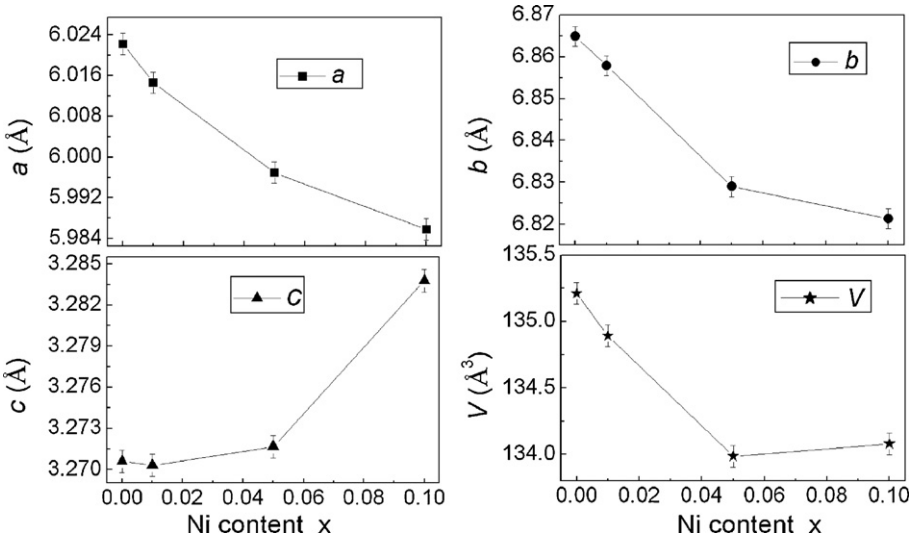

Fig. 2. Composition (x) dependence of lattice parameters a, b, c and volume of unit cell V for $Cr_{1-x}Ni_xSb_2$ (x = 0, 0.01, 0.05, and 0.10) at room-temperature.

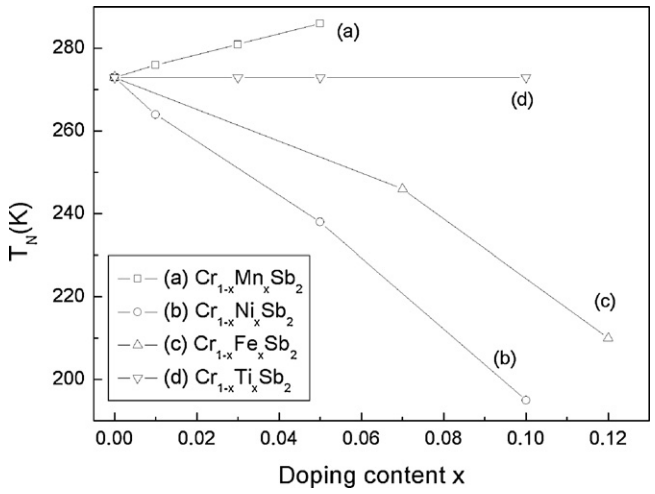

Fig. 4. Plot of Neel temperatures T_N versus doping content x for $Cr_{1-x}Mn_xSb_2$, $Cr_{1-x}Ni_xSb_2$, $Cr_{1-x}Fe_xSb_2$ and $Cr_{1-x}Ti_xSb_2$.

cessfully substituted for Cr, leading to formation of $Cr_{1-x}Ni_xSb_2$ compounds.

3.2. Electrical resistivity and thermopower

Fig. 3 shows the temperature dependence of the electrical resistivity (plotted as $\ln\rho$ versus T) for $Cr_{1-x}Ni_xSb_2$ at temperatures ranging from 7 to 310 K. All of the samples exhibit semiconductor-like behavior, and the resistivity ρ decreases substantially with increasing Ni content below ~100 K, however, the resistivity of $Cr_{0.99}Ni_{0.01}Sb_2$ and $Cr_{0.95}Ni_{0.05}Sb_2$ is larger than that of $CrSb_2$ above ~150 K. In addition, a plateau and a marked anomaly are observed in the $\ln\rho$–T curve of $CrSb_2$ (Fig. 3), which is well consistent with previous results [34,38]. By comparing curve (a) with curves (b)–(d) in Fig. 3, one can see that the plateau is effectively prohibited by Ni substitution, and the Neel temperature T_N decreases from 273(±2) K for $x = 0$ to 264(±2) K for $x = 0.01$, 238(±2) K for $x = 0.05$, and 195(±2) K for $x = 0.10$ (Fig. 4(b)) due to the substitution of low spin Ni ($3d^6$) for high spin Cr ($3d^2$), leading to a reduction in the effective moment of Cr in $CrSb_2$, which is similar to Fe doped compounds [32,35], but different from Mn-doped compounds [40], the substitution of high spin Mn ($3d^3$) for Cr with one more unpaired electron leads to the increase in Neel temperature.

In order to examine the temperature behavior of the resistivity for $Cr_{1-x}Ni_xSb_2$, logarithm of resistivity $\ln\rho$ is plotted as a function of T^{-1} in Fig. 5. Their resistivity can be expressed using a thermally activated form in the corresponding temperature regions, written as:

$$\rho = \rho_0 \exp\left(\frac{\Delta E}{k_B T}\right) \quad (1)$$

where ρ_0 is the pre-exponential factor, ΔE is the activation energy for conduction, and k_B is the Boltzmann constant. The best fit of the experimental data to Eq. (1) yields four activation energies ΔE_i (i = 1–4) for $CrSb_2$: 32.6 (~276 K < T < ~310 K), 35.7 (~60 K < T < ~276 K), 4.6 (~12 K < T < ~60 K), and 0.9 meV (~7 K < T < ~12 K), respectively. The value of ΔE_2 is about half of the energy gap (E_g), or 0.07 eV, which is larger than ΔE_1 for $CrSb_2$, possibly caused by the transition from anti-ferromagnetism to paramagnetism. However, ΔE_3 and ΔE_4 are much smaller than ΔE_2 (or the E_g), indicating that they could be attributed to impurity or defect levels. The decrease of activation energies ΔE_i (Fig. 6)

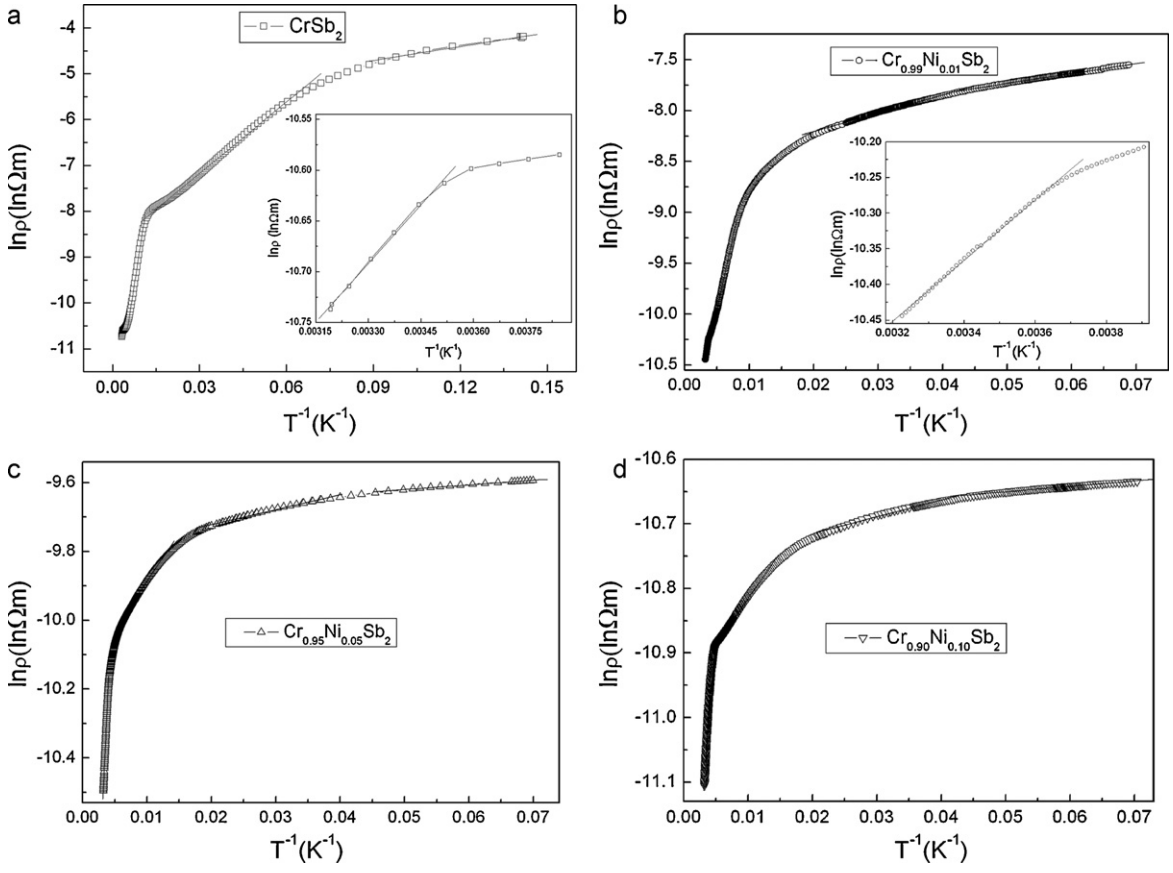

Fig. 5. Plot of $\ln\rho$ versus T^{-1} for $Cr_{1-x}Ni_xSb_2$ (x = 0, 0.01, 0.05, and 0.10).

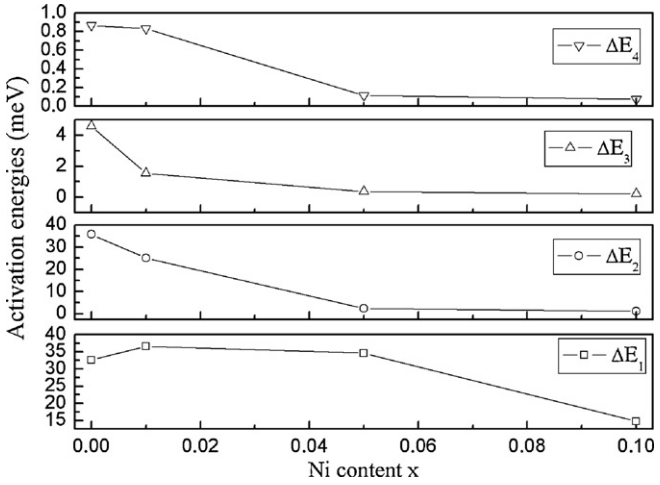

Fig. 6. Variation of the activation energies ΔE_i (i = 1–4) with the Ni content x for $Cr_{1-x}Ni_xSb_2$.

Table 1
Hall coefficent R_H, carrier contention n_c, and resistivity ρ of $Cr_{1-x}Ni_xSb_2$ ($0 \le x \le 0.10$) at room temperature.

Composition (x)	0	0.01	0.05	0.10
R_H ($cm^3\,C^{-1}$)	−0.48	−0.59	−0.56	−0.25
n_c ($\times 10^{21}\,cm^{-3}$)	1.31	1.06	1.11	2.54
ρ ($\times 10^{-5}\,\Omega m$)	2.31	3.16	2.74	1.13

suggests that a shift in impurity or defect levels toward the edge of conduction band(s), or even a narrowing of the energy gap would occur due to lattice distortion after doping (Fig. 2), which is well consistent with previous results [39,41]. On the other hand, the donor level could be introduced into the energy gap of $CrSb_2$ after Ni substitution. As a result, both of the factors could lead to an increase in electron concentration, in agreement with the decrease in resistivity after Ni doping at $T < \sim 100$ K. Furthermore, the electron concentration calculated from measurements of the R_H at room temperature is $1.31 \times 10^{21}\,cm^{-3}$ for $x = 0$, $1.06 \times 10^{21}\,cm^{-3}$ for $x = 0.01$, $1.11 \times 10^{21}\,cm^{-3}$ for $x = 0.05$, and $2.54 \times 10^{21}\,cm^{-3}$ for $x = 0.10$ (Table 1), which could explain the observed variation in the resistivity of $Cr_{1-x}Ni_xSb_2$ above ~150 K (Fig. 3).

Fig. 7 gives thermopower as a function of temperature for $Cr_{1-x}Ni_xSb_2$. The thermopower for all the samples is negative,

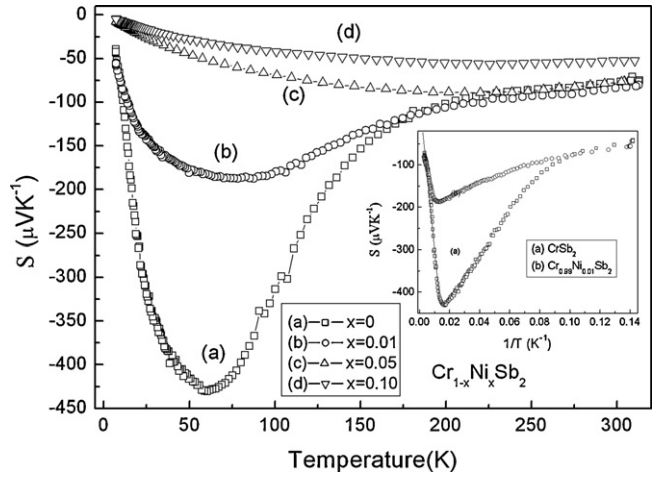

Fig. 7. Variation of thermopower S with temperature T for $Cr_{1-x}Ni_xSb_2$ (x = 0, 0.01, 0.05, and 0.10). The inset shows the variation of thermopower S with T^{-1} for the $Cr_{1-x}Ni_xSb_2$ (x = 0, 0.01).

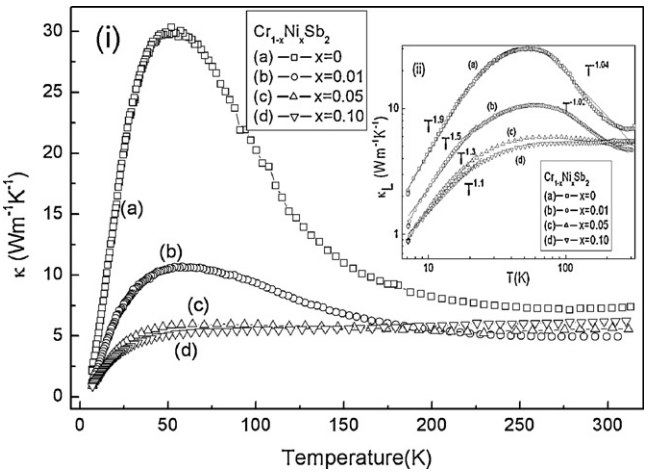

Fig. 8. Variation of thermal conductivity κ(i) and lattice thermal conductivity κ_L(ii) with temperature T for $Cr_{1-x}Ni_xSb_2$ (x = 0, 0.01, 0.05, and 0.10)

indicating that the major charge carriers are electrons in those compounds over the entire temperature range. A large peak is observed in the curve of S–T for $CrSb_2$ at ~60 K (Fig. 7), which corresponds to the plateau in the $\ln \rho$ versus T curve, and is also related to the electronic change of the electron-spin system. It can be seen from Fig. 7 that $|S|$ decreases with increasing Ni content in the whole temperature range due to an increase in the electron concentration caused by the substitution of Ni for Cr; while the disappearance of the peak in the curves of S–T (Fig. 7) could originate from the suppression of the electronic change of the electron-spin system, which is in agreement with the elimination of the plateau in the curves of $\ln \rho$–T (Fig. 3). In addition, the thermopower $|S|$ of $CrSb_2$ and $Cr_{0.99}Ni_{0.01}Sb_2$ could be expressed as the sum of a temperature independent term and a temperature dependent term [45]:

$$S = S_0 + \frac{k_B}{|e|}\frac{E_s}{k_B T} \quad (2)$$

where E_s is a characteristic energy for S, and S_0 is the thermopower in the high-temperature limit. The best fit of the experimental data to Eq. (2) yields two values of E_s: 35.7 meV and 15.9 meV for $CrSb_2$ and $Cr_{0.99}Ni_{0.01}Sb_2$, respectively. The characteristic energy E_s (=35.7 meV) for $CrSb_2$ is equal to the activation energy ΔE_2 (=35.7 meV), suggesting that $CrSb_2$ is an intrinsic non-degenerate semiconductor. In the case of $Cr_{0.99}Ni_{0.01}Sb_2$, E_s (=15.9 meV) is smaller than ΔE_2 (=25.4 meV), indicating that the Fermi level E_F is higher than impurity level E_2.

3.3. Thermal conductivity and figure of merit

Fig. 8(i) presents the total thermal conductivity (κ) as a function of temperature for $Cr_{1-x}Ni_xSb_2$. A maximum value of thermal conductivity for $CrSb_2$ and $Cr_{0.99}Ni_{0.01}Sb_2$ appears in the curve of κ–T. In contrast, the thermal conductivity of $Cr_{0.95}Ni_{0.05}Sb_2$ and $Cr_{0.9}Ni_{0.1}Sb_2$ shows weak temperature dependence in the temperature range from 50 to 310 K. The total thermal conductivity (κ) may be expressed as the sum of the lattice component (κ_L) and the carrier component (κ_C): $\kappa = \kappa_L + \kappa_C$. The κ_C values can be estimated from the Wiedemann–Franz's law as $\kappa_C = L_0 T/\rho$, where L is the Lorentz number and ρ is the electrical resistivity. As a semi-quantitative estimation, we use the value L_0 of free electrons for L (i.e. $L = L_0 = 2.44 \times 10^{-8}\,V^2\,K^{-2}$) for all the samples. Consequently, the lattice thermal conductivity (κ_L) can be obtained from κ and κ_C, as shown in Fig. 8(ii). By comparing Fig. 8(i) with (ii), it can be seen that the thermal conductivities of all compounds arise

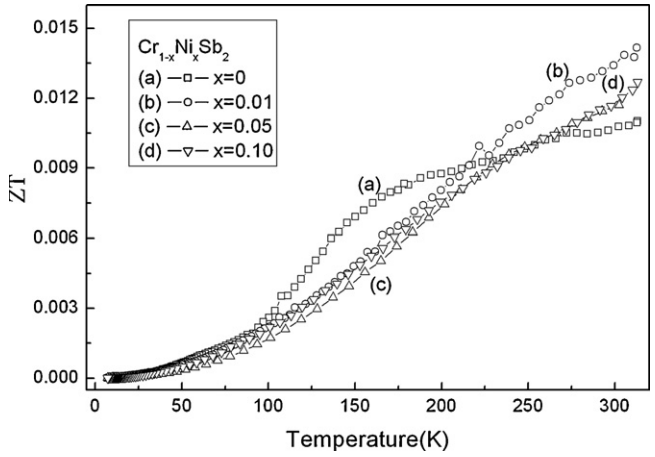

Fig. 9. Variation of ZT with temperature T for $Cr_{1-x}Ni_xSb_2$ ($x = 0, 0.01, 0.05$, and 0.10).

mainly from their lattice thermal conductivities. As compared to that of $CrSb_2$, the thermal conductivity of the doped compounds decreases from 30.3 W m^{-1} K^{-1} for $x = 0$–5.1 W m^{-1} K^{-1} for $x = 0.1$ at ~50 K. This large and continuous decrease of low-temperature thermal conductivity could be ascribed to the enhancement of the phonon scattering by impurity (Ni) atoms. Fig. 8(ii) gives the lattice thermal conductivity (κ_L) as a function of T^a for $Cr_{1-x}Ni_xSb_2$ at low temperatures ($T < 30$ K). By the best fit of the experimental data one obtains $a = 1.9$ for $x = 0$, 1.5 for $x = 0.01$, 1.3 for $x = 0.05$, and 1.1 for $x = 0.1$, respectively. The power law of $\kappa_L \propto T^{1.9}$ for $CrSb_2$ suggests that both point-defects and grain-boundaries contribute to the scattering for temperatures down to 7 K. However, the dependence $\kappa_L \propto T^{1.1}$ for $Cr_{0.9}Ni_{0.1}Sb_2$ is a strong indication of the presence of electron–phonon interaction [46]. According to the usual phononic heat transport theory, the relationship between lattice thermal conductivity and temperatures above ~30 K can be written as $\kappa_L \propto T^n$ (Fig. 8(ii)), and the values of n are −1.04 and −1.02 for $CrSb_2$ and $Cr_{0.99}Ni_{0.01}Sb_2$, respectively. The results indicate that the values of n are basically equal to −1 within the experimental errors, suggesting that phonon–phonon interactions are the primary source of thermal resistance.

The figure of merit ZT values of $Cr_{1-x}Ni_xSb_2$ is calculated and presented as a function of temperature in Fig. 9. The ZT values for all the samples increase monotonically with increasing temperature. Above approximately ~250 K, the ZT values of doped compounds are noticeably larger than those of $CrSb_2$. Specifically, the ZT value for $Cr_{0.99}Ni_{0.01}Sb_2$ is about 0.014 at 310 K, which is about 29% larger than that of $CrSb_2$, indicating that thermoelectric properties of $CrSb_2$ could be improved by proper substitution of Ni for Cr.

4. Conclusions

Substituted compounds $Cr_{1-x}Ni_xSb_2$ were synthesized, and the effect of Ni substitution on the transport and thermoelectric properties of $Cr_{1-x}Ni_xSb_2$ were investigated at the temperatures below 310 K. The results indicated that electrical resistivity (ρ) and thermopower ($|S|$) of $Cr_{1-x}Ni_xSb_2$ decreased greatly with increasing Ni content due to an increase in electron concentration caused by Ni substitution for Cr. In addition, experiments shown that low-temperature lattice thermal conductivity of $Cr_{1-x}Ni_xSb_2$ decreased substantially with increasing Ni content, presumably due to enhanced phonon scattering by doped Ni atoms. Moreover, the ZT value of $Cr_{0.99}Ni_{0.01}Sb_2$ is about 0.014 at 310 K, indicating that the thermoelectric properties of $CrSb_2$ could be improved by proper substitution of Ni for Cr. Furthermore, the Neel temperature of $Cr_{1-x}Ni_xSb_2$ decreased from 273 K for $CrSb_2$ to 195 K for $Cr_{0.9}Ni_{0.1}Sb_2$, which may be caused by the substitution of the low spin state Ni ($3d^6$) for a high spin state Cr ($3d^2$), weakening the effective moment of doping compounds.

Acknowledgements

Financial support from National Natural Science Foundation of China (Grants Nos. 10774145, 50701043, 10904144, 50972146 and 50701002) is gratefully acknowledged.

References

[1] F.J. DiSalvo, Science 285 (1999) 703.
[2] C.-N. Liao, L.-C. Wu, L.-C. Lee, J. Alloys Compd. 490 (2010) 468.
[3] C.-H. Kuo, C.-S. Hwang, M.-S. Jeng, W.-S. Su, Y.-W. Chou, J.-R. Ku, J. Alloys Compd. 496 (2010) 687.
[4] Y.S. Hor, R.J. Cava, J. Alloys Compd. 479 (2009) 368.
[5] C.D. Moon, S. Shin, D.H. Kim, T.-S. Kim, J. Alloys Compd. 504 (2010) S504.
[6] J.J. Shen, S.N. Zhang, S.H. Yang, Z.Z. Yin, T.J. Zhu, X.B. Zhao, J. Alloys Compd. 509 (2011) 161.
[7] T.-S. Su, X. Jia, H. Ma, J. Guo, Y. Jiang, N. Dong, L. Deng, X. Zhao, T. Zhu, C. Wei, J. Alloys Compd. 468 (2009) 410.
[8] K.F. Cai, C. Yan, Z.M. He, J.L. Cui, C. Stiewe, E. Müller, H. Li, J. Alloys Compd. 469 (2009) 499.
[9] T. Su, S. Li, S. Ma, X. Li, L. Deng, Y. Yan, W. Guo, X. Jia, J. Alloys Compd. 497 (2010) 432.
[10] J.H. Sun, X.Y. Qin, H.X. Xin, D. Li, L. Pan, C.J. Song, J. Zhang, R.R. Sun, Q.Q. Wang, Y.F. Liu, J. Alloys Compd. 500 (2010) 215.
[11] W. Li, L.M. Zhou, Y.L. Li, J. Jiang, G.J. Xu, J. Alloys Compd. 486 (2009) 335.
[12] L. Pan, X.Y. Qin, M. Liu, F. Liu, J. Alloys Compd. 489 (2010) 228.
[13] L.M. Zhou, W. Li, J. Jiang, T. Zhang, Y. Li, G.J. Xu, P. Cui, J. Alloys Compd. 503 (2010) 464.
[14] P.-J. Lee, S.C. Tseng, L.-S. Chao, J. Alloys Compd. 496 (2010) 620.
[15] M. Mikami, S. Tanaka, K. Kobayashi, J. Alloys Compd. 484 (2009) 444.
[16] P.-J. Lee, L.-S. Chao, J. Alloys Compd. 504 (2010) 192.
[17] M. Chitroub, F. Besse, H. Scherrer, J. Alloys Compd. 467 (2009) 31.
[18] L. Zhang, A. Grytsiv, M. Kerber, P. Rogl, E. Bauer, M. Zehetbauer, J. Alloys Compd. 490 (2010) 19.
[19] L. Zhang, N. Melnychenko-Koblyuk, E. Royanian, A. Grytsiv, P. Rogl, E. Bauer, J. Alloys Compd. 504 (2010) 53.
[20] L.X. Xu, F. Li, Y. Wang, J. Alloys Compd. 501 (2010) 115.
[21] J. Liu, C.L. Wang, W.B. Su, H.C. Wang, J.C. Li, J.L. Zhang, L.M. Mei, J. Alloys Compd. 492 (2010) L54.
[22] N. Wang, H.C. He, X. Li, L. Han, C.Q. Zhang, J. Alloys Compd. 506 (2010) 293.
[23] S. Pinitsoontorn, N. Lerssongkram, A. Harnwunggmoung, K. Kurosaki, S. Yamanaka, J. Alloys Compd. 503 (2010) 431.
[24] H.F. Wang, K.F. Cai, H. Li, D.H. Yu, X. Wang, C.W. Zhou, X.L. Li, Y.Y. Wang, B.J. An, Y. Du, J. Alloys Compd. 491 (2010) 684.
[25] Y. Saiga, K. Suekuni, S.K. Deng, T. Yamamoto, Y. Kono, N. Ohya, T. Takabatake, J. Alloys Compd. 507 (2010) 1.
[26] I. Terasaki, Y. Sasago, K. Uchimokuro, Phys. Rev. B 56 (1997) R12685.
[27] ParkF C.-M., H.-J. Sohn, Electrochim. Acta 55 (2010) 4987.
[28] F.J. Fernaïndez-Madrigal, P. Lavela, C. Peïrez-Vicente, J.L. Tirado, J. Electroanal. Chem. 501 (2001) 205.
[29] H.J. Li, X.Y. Qin, D. Li, Mater. Sci. Eng. B: Solid 149 (2008) 53.
[30] G. Brostigen, A. Kjekshus, Acta Chem. Scand. 24 (1970) 2983.
[31] K. Adachi, K. Sato, M. Matsuura, J. Phys. Soc. Jpn. 26 (1969) 906.
[32] G. Brostigen, A. Kjekshus, Acta Chem. Scand. 24 (1970) 2993.
[33] J.B. Goodenough, J. Solid State Chem. 5 (1972) 144.
[34] H. Holseth, A. Kjekshus, Acta Chem. Scand. 24 (1970) 3309.
[35] A. Kjekshus, P.G. Peterzens, T. Rakke, A.F. Andresen, Acta Chem. Scand. Ser. A 33 (1979) 469.
[36] T. Harada, Y. Takahashi, Y. Yamaguchi, T. Kanomata, H. Yoshida, T. Kaneko, Y. Kawazoe, J. Magn. Magn. Mater. 310 (2007) 1569.
[37] Y. Takahashi, T. Harada, T. Kanomata, K. Koyama, H. Yoshida, T. Kaneko, M. Motokawa, M. Kataoka, J. Alloys Compd. 459 (2008) 78.
[38] T. Harada, T. Kanomata, Y. Takahashi, O. Nashima, H. Yoshida, T. Kaneko, J. Alloys Compd. 383 (2004) 200.
[39] H.J. Li, X.Y. Qin, D. Li, H.X. Xin, J. Alloys Compd. 472 (2009) 400.
[40] H.J. Li, X.Y. Qin, D. Li, J. Alloys Compd. 467 (2009) 299.
[41] H.J. Li, X.Y. Qin, Y. Liu, D. Li, J. Alloys Compd. 506 (2010) 917.
[42] H. Holseth, A. Kjekshus, Acta Chem. Scand. 22 (1968) 3284.
[43] A. Kjekshus, T. Rakke, A.F. Andresen, Acta Chem. Scand. 28 (1974) 996.
[44] E. Bjerkelund, A. Kjekshus, Acta Chem. Scand. 24 (1970) 3317.
[45] T.T.M. Palstra, A.P. Ramirez, S.W. Cheong, B.R. Zegarski, P. Schiffer, J. Zaanen, Phys. Rev. B 56 (1997) 5104.
[46] J. Yang, D.T. Morelli, G.P. Meisner, W. Chen, J.S. Dyck, C. Uher, Phys. Rev. B 65 (2002) 094115.